

Chapter 22

Morphology and Fatigue Behaviour of Short-Glass Fibre-Reinforced Polypropylene

M. Palmstingl, D. Salaberger and T. Koch

Abstract The fatigue behaviour of short-glass fibre-reinforced polypropylene was investigated in dependence on the fibre orientation. For that, a special plate geometry was developed which allows to exclude the effect of machining and leads to original injection surfaces at least in the region of the main (slightly concentrated) load. This “original” surface matches the surface situation of the injection moulded consumer parts. Furthermore, the plates consist of a notch region and a knit line. Morphology analysis can be done by sectioning and stereological principles or by X-ray computed tomography. The fatigue strength shows a strong correlation to fibre orientation, but the samples taken from the knit line and the notch region do not follow this correlation. In these regions the situations are more complex. The application of different methods for the characterization of the evolution of damage (development of dissipated energy, strain, normalized modulus, temperature) does not give a clear indication of damage; there are no clear signs of damage until shortly before the fracture. High-speed camera in combination with digital image correlation can give information on local strain and therefore on the localized occurrence of damage at a relatively early stage of fatigue life.

22.1 Introduction

The wide use and growing of industrial applications of short fibre-reinforced polymers (SFRP) has different reasons: low manufacturing costs, high production rate, good weight to stiffness and strength ratio and the possibility to mould it into complex shapes. In practice plastic components and constructions are often subject of cyclic loading which is one major reason of mechanical failures. Cyclic loading can lead to fatigue failure at essentially lower stresses or deformations than under

M. Palmstingl (✉) · T. Koch
Institute of Materials Science and Technology,
Vienna University of Technology, Vienna, Austria

D. Salaberger
University of Applied Sciences of Upper Austria, Wels, Austria

quasi-static loading conditions. Damages arise already in the region of linear-viscoelastic materials behaviour. The loading conditions are often very complex. Orientations, agglomerations, notches, weld lines, environmental conditions are factors influencing the fatigue failure. So, it is important to consider these parameters in fatigue testing. Also, all these things mean that a comprehensive description of mechanical materials or component behaviour requires—besides quasi-static, impact and creep testing—also fatigue testing.

A good overview about results on fatigue behaviour of polymeric materials is given in [1], a literature review on short fibre-reinforced polymers can be found in [2]. The most investigations were done on short fibre-reinforced polyamides [3–10] reflecting the fact that these thermoplastic materials are the most widely used matrix polymers of SFRPs in industrial applications. Investigations on SFR polypropylene are presented in [11–14].

It is well known that the orientations of the fibres have a large impact on the fatigue behaviour and all the test results cannot be assessed without the knowledge of the morphology of the composites. The morphology can be described by microscopy or X-ray tomography. Both methods need some efforts to receive adequate results.

To model the damage accumulation and predict the fatigue life different mechanical parameters are used in literature. They are mostly based on the dissipative response, for example on the progression of hysteresis loop, strain energy, non-linear viscoelasticity or hysteretic energy [2].

22.2 Analysis of Morphology of SFRP

Morphological characterisation provides fundamental information about the properties and behaviour of polymer composites. Since the microstructure of such composite materials highly affects bulk material properties, the prediction of morphological structures by simulation is of considerable interest for the designing of industrial applications. For the validation of moulding simulation models commonly morphological investigation methods like microscopic or tomographic techniques are used [15].

X-ray Computed Tomography (X-CT) (Fig. 22.1) is currently the most appropriate method to describe the morphology of short fibre-reinforced polymers, which is reflected by an increasing number of works in the literature. Fibre content, fibre orientation, fibre length distribution and the local 3-dimensional distribution of the three parameters can be obtained. Applying suitable segmentation methods is an essential requirement to extract correct quantitative morphology parameters from X-CT [16]. Especially agglomerates of fibres could influence the results, namely the calculated length distribution. With the onward development of equipment and software X-CT will become the standard for the investigation of polymer composites. At the moment the limiting factor are mainly the high costs of the devices or of contract measurements.

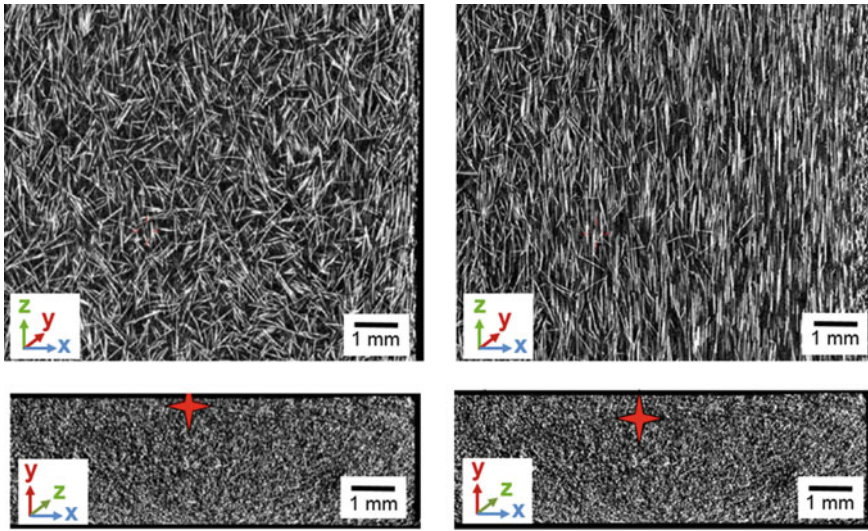


Fig. 22.1 Example of X-CT results on SFRP. Visualisation of fibre arrangement in different planes. *Z* injection direction, *Y* thickness direction. The stars indicate the position of the above shown X-*Z*-plane

Stereological principles are basic considerations for the analysis of microstructures with microscopic investigations of polished cut surfaces [17]. Although other methods were used frequently [18–22], the sectioning of fibre-reinforced polymers followed by light microscopic investigations and digital image analysis is still the most commonly used technique for the determination of the distribution of fibre orientation [23–28]. The relative simplicity of the required measurement setup, particularly compared with non-destructive techniques like tomographic ones, let this method be preferred even though it must be considered, that there are inaccuracies in the model [29, 30].

The theory bases on the optical observation of elliptical marks occurring by the intersection of cylindrical reinforcement materials like fibres. Polishing sections from a sample leads to such elliptical fibre marks due to the cutting of the cylindrical fibres. The two polar angles ϕ and θ , that define the orientation of the fibre, can be determined from the footprint of each fibre. The angle θ thereby defines the angle between the fibres longitudinal axis and the sectioned surface normal (22.1), whereby b is defined as the ellipses minor half axis and a as the ellipses major half axis. The second polar angle ϕ defines the angle between the major axis of the elliptical fibre mark and one of the in-plane axes (see Fig. 22.2).

$$\theta = \cos^{-1}\left(\frac{b}{a}\right) \tag{22.1}$$

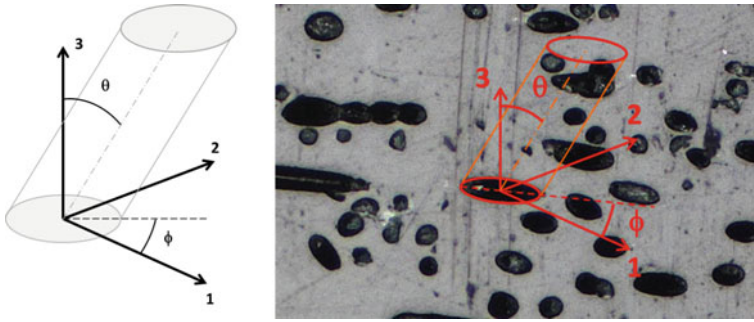


Fig. 22.2 The fibre orientation defined by means of the two polar angles ϕ and θ theoretically (*left*) and applied on a sample (*right*)

An example for the investigation of one of the observed plate positions is shown in Fig. 22.3. The location on the plate is called 0° -position. In Fig. 22.3b a high amount of fibres with a polar angle ϕ around 90° (parallel to axis 2) is already obvious and can also be confirmed through the analysis, shown in Fig. 22.3d. Regarding polar angle θ , fibres at this plate position are orientated either 0° or in the range of 70° – 90° . These calculated results (Fig. 22.3e) are again evident by interpreting the visible fibres in Fig. 22.3b. The almost circular appearing fibre marks represent an angle of 0° whereas the partially quite long ellipses illustrate the angles of 70° – 90° for θ .

Subsequently, the results of the so-called 90° -position on the plate (Fig. 22.4) can be concluded logically. The angle ϕ shows a quite equal distribution (Fig. 22.4d). There is no predominant “in plane”-orientation, which can also be recognised in the surface cuts of the different planes presented in Fig. 22.4b. The results of the polar angle θ (Fig. 22.4e) are very similar to the ones of the 0° -position.

The calculation of the two polar angles enables the determination of the orientation of a single fibre by expressing it as a second order orientation tensor a_{ij} . The calculation and a detailed discussion about the formation and application about orientation tensors can be found elsewhere [32]. The orientation of an individual fibre is defined by the main diagonal components of the tensor that are given in the following equations (22.2) [32].

$$\begin{aligned} a_{11} &= \sin^2 \theta \cdot \cos^2 \phi \\ a_{22} &= \sin^2 \theta \cdot \sin^2 \phi \\ a_{33} &= \cos^2 \theta \end{aligned} \quad (22.2)$$

The fibre orientation of an investigated sample is then given by the average of the single fibre orientation. For an unbiased estimation of the orientation tensor, the tensor components must be weighted for each fibre. Therefore the inverse of the probability of intersecting each fibre must be included. This weighted orientation tensor is described in earlier publications [26, 29].

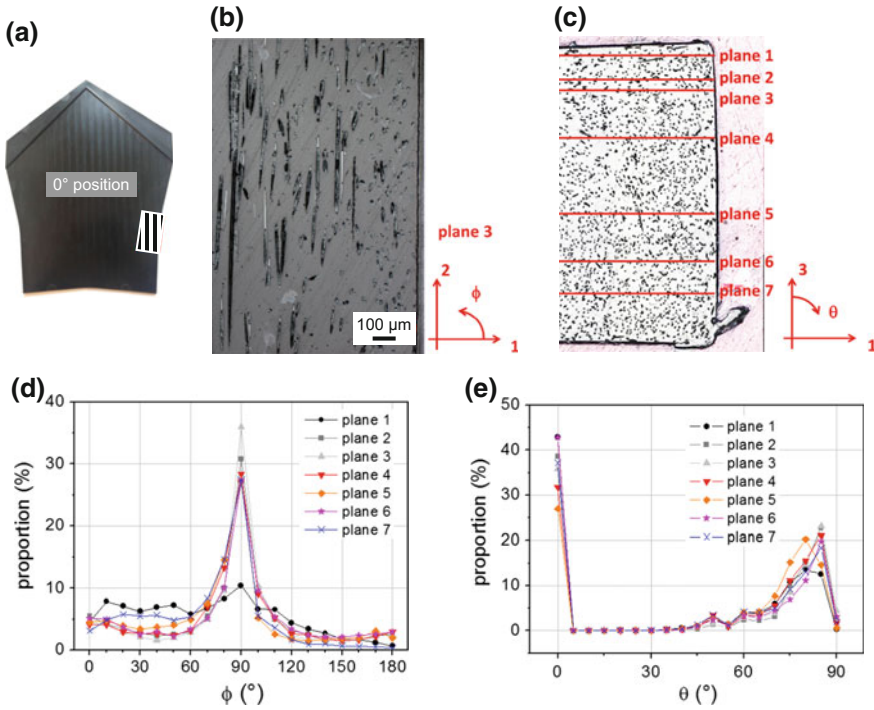


Fig. 22.3 The plate form and the labelled position (a), polished cut surface from 0°-position on plane 3 (b), plate cross section with marking of all investigated plane positions (c), distribution of polar angle ϕ in dependency of the sample planes (d), distribution of polar angle θ in dependency of the sample planes (e) [31]

For the presented examples of the 0°- and 90°-position (Figs. 22.3 and 22.4), Table 22.1 gives the calculated main diagonal components of the weighted orientation tensor. The polar angles distributions are reflected suitable through the calculated results of the microscopic analysis.

The contrast between glass fibres and the matrix material is usually inadequate for an automatic data analysis following a reflecting light microscopic investigation. Because of the poor contrast of glass fibres as well as the contrast dependence on different sample preparation parameters like the polishing procedure or the polishing time, there has to be a contrast enhancement prior to the optical image generation. Commonly used are etching approaches, where glass fibres were dissolved and the remaining holes, representing the originally existing fibres, will be analysed instead. For the etching procedure oxygen ions can be used [33, 34]. Figure 22.5 shows the difference between etched and untreated samples, whereby hydrofluoric acid was used as etching agent in this case.

Another major morphological characteristic of fibre-reinforced polymers is the average fibre length. There are approaches to determine an average fibre length from cross-sectional data by an indirect calculation, where the number of

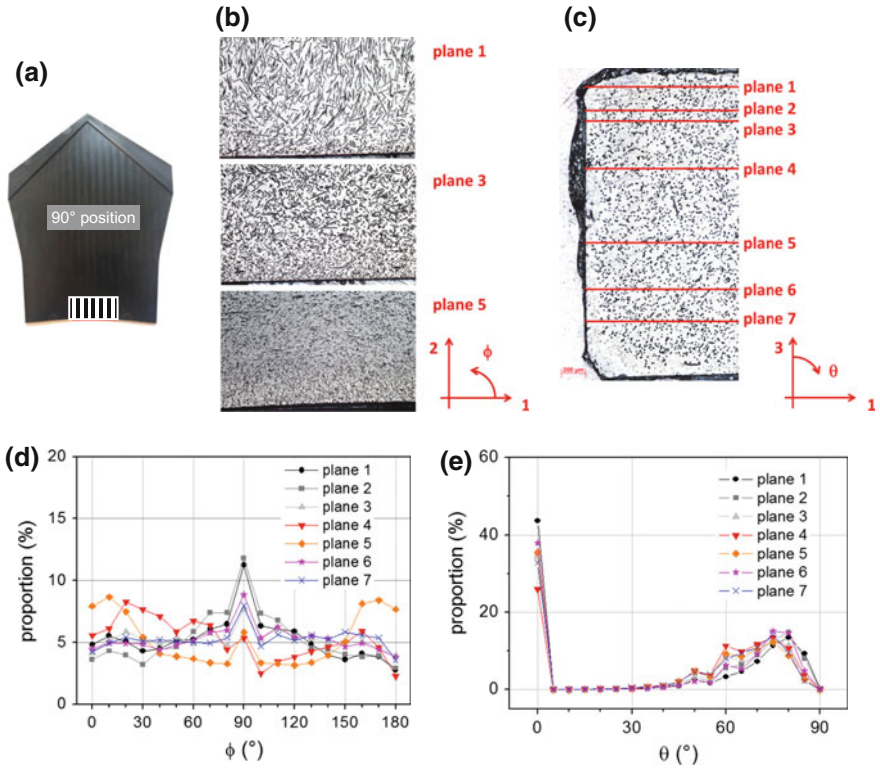


Fig. 22.4 The plate form and the labelled position (a), polished cut surface from 90°-position on planes 1, 3 and 5 (b), plate cross section with marking of all investigated plane positions (c), distribution of polar angle ϕ in dependency of the sample planes (d), distribution of polar angle θ in dependency of the sample planes (e) [31]

Table 22.1 Main diagonal components of the weighted orientation tensor calculated from the surface cuts after the microscopic analysis

Tensor component	0°-position	90°-position
a_{11}	0.053	0.191
a_{22}	0.304	0.162
a_{33}	0.643	0.647

intersected fibre ends on a cross-section image provides information for the estimation of the average fibre length [35]. Inaccuracies in the estimations lead to the two-section method, an approach, where two consecutive closely-spaced parallel cross-sections of a specimen provide a more precise estimation of the average fibre length directly from microscopic images after sectioning [36]. These images have to be transformed into a black and white image before a software tool can identify the related fibre ellipses in the two images of the same area but different closely-spaced planes. Figure 22.6 demonstrates the transformation of microscopic images into black and white images of the different planes and a superposition of both sections.

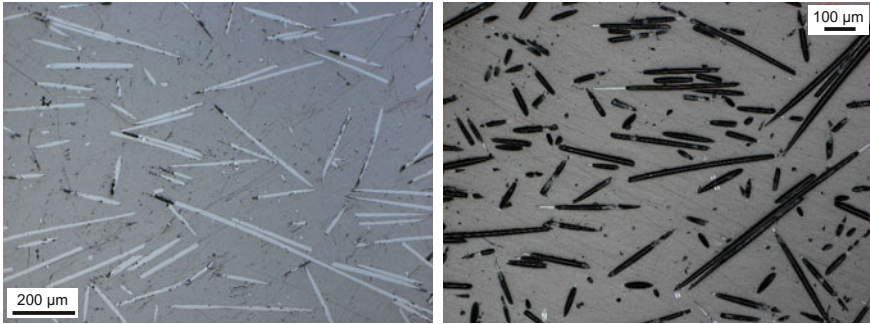


Fig. 22.5 Polished cut surfaces without etching (*left*) and etched (*right*)

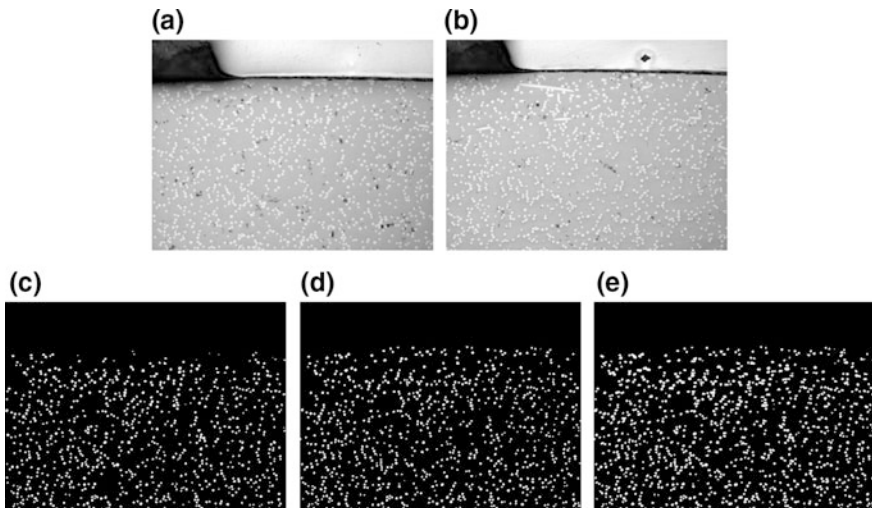


Fig. 22.6 Images generated for the two-section method: microscopic image of the upper plane (a), microscopic image of the lower plane (b), transformed black and white image of the upper plane (c), transformed black and white image of the lower plane (d), superposition of the black and white images of the two sections (e) [31]

A single fibre can be seen in either one or both planes. The superposition connects the two sections so that the fibres can be identified in both planes as the same fibre. The average fibre length can be estimated by using statistical analysis under the consideration of the distance between the planes and the probability that a fibre with a certain length has to cross both sections.

Another attempt to correct the estimated average fibre length as well as a method to determine the real fibre length distribution from measured lengths of the fibres from cross-section images is proposed elsewhere [30].

Besides the analysis of cross-sectional images, actually there are other destructive and non-destructive methods to measure the fibre length. Commonly used are methods, where the fibre length can be directly measured after the burnout or dissolution of the polymer [36, 37]. Hereby the remaining fibres after an ashing procedure at high temperatures are measured by means of image analysis and optical microscopy.

Figure 22.7 shows such a microscopic image. After the burnout of the polypropylene matrix at a temperature of 530 °C and a dwell time of 1.5 h, the remaining glass fibres were floated with ethanol. Then, random samples were drawn from the population and investigated with reflected light microscopy. The length of each single fibre is determined easily by directly measuring the observable length.

The fibre length as well as the fibre orientation distribution furthermore can be determined by Computed Tomography (CT) [16, 38, 39]. Thereby, a series of radiographic projections are taken at different angles. The internal structure of a sample is then reconstructed using an algorithm for combining the generated projections information. With an appropriate resolution and specific data evaluation concepts, the starting and end points of single fibres can be extracted and thus fibre characteristics like the fibre length and orientation determined [16].

Even though there are correction approaches for most of the methods, the summary of the determined fibre lengths, obtained with different investigation methods, in Table 22.2 shows an analogy of the CT and ashing result. The two-section method produced unsatisfactorily and unequal results.

Fig. 22.7 Drawn sample of fibres after burnout

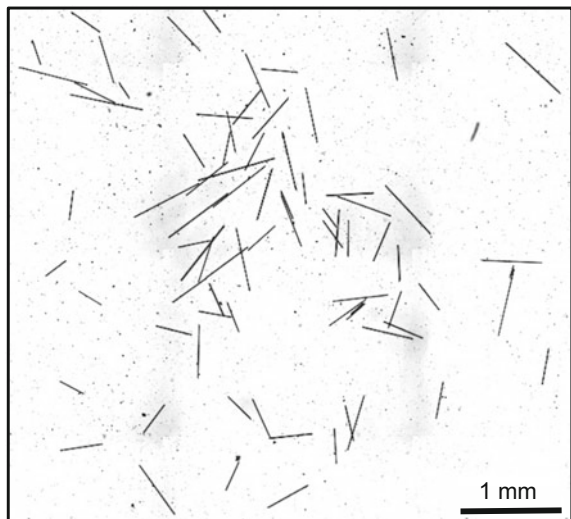


Table 22.2 Determined fibre lengths obtained with different investigation methods

Method	No. of investigated fibres	Mean fibre length (µm)	Standard deviation (µm)
Two-section method	8101	233.7	68
Ashing	1541	293.4	6
CT	31,368	309.8	3

22.3 Determination of Fatigue Behaviour

The knowledge of the real existing fibre orientation is essential for the rating of investigation results for mechanical parameter like tensile strength or fatigue behaviour. Also the general known effect of a reduction in fibre length during processing [40] particularly of short fibre-reinforced polymers, which is not included in usual simulations, justifies the experimental investigation of morphological characteristics. The results of tensile tests, fatigue testing and durability analysis are then correlated with morphological characteristics and both are the basis for later executed simulations for fatigue behaviour and crack initiation.

Typically, specimens with different fibre orientations were machined from injection moulded plates with different angles of the specimen main axis to the injection direction. That means that the machined surfaces can influence the results obtained by fatigue testing. To exclude this possible effect it makes sense to produce specimens with original injection surfaces at least in the region of the main (concentrated) load. This “original” surface matches the surface situation of the injection moulded consumer parts.

For all subsequent investigations, the prepared specimens were taken from the three different injection moulded plate forms in two different types. The “standard” specimens were sampled from the positions of the plates, shown in Fig. 22.8.

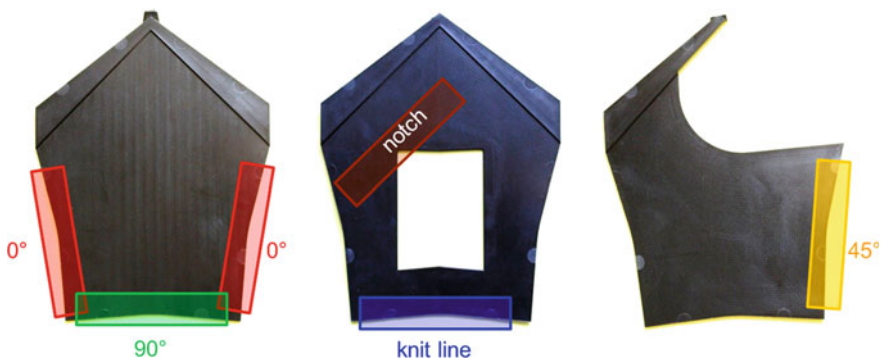


Fig. 22.8 Positions of the “standard” specimens prepared from the different plates

Only the 45°-specimen of the plate form with the eccentric inset was not considered satisfactory of its morphological properties and was not investigated henceforth. Figure 22.9 shows the dimensions of some of the other specimen positions. The special feature of this kind of preparation is the realisation of a little stress concentration as a consequence of the concave rounding of the specimen. Thus a defined area to locate the loading could be achieved for a targeted observation.

During the testing, it figured out, that the intended orientation of the “standard” specimen did not coincide with the analysed orientations from the morphological analysis in a satisfactory manner for some of the positions (Table 22.3). Though, a high degree of fibre orientation in combination with the belonging mechanical characteristics is required for satisfying simulation results. Therefore the “mini” specimens, the second types of prepared specimens, were intended. Due to the smaller area of the “mini” specimen a higher degree of orientation is reachable.

It turned out, that the highest degree of orientation could be achieved through the preparation of “mini” specimen from the testing plate with the centric inset. It is also the only plate form, where all for the simulation relevant kind of fibre orientations appear. Figure 22.10 shows the locations and positions of the places of sampling, the dimensions and also how these specimen types could be mounted in the testing machine.

The higher degree of orientation is clearly visible in Fig. 22.11. The 0°-position and the 90°-position obviously mirror them and show evidently a higher degree of orientation compared to the “standard” specimen. Due to the elaborated selection of the preparation positions no distinct layer constructions appeared. Table 22.4 shows

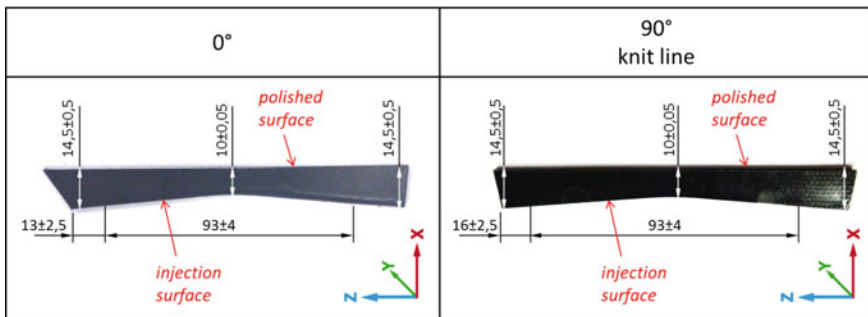


Fig. 22.9 Prepared “standard” specimen for 0°, 90° and knit line

Table 22.3 Main diagonal components of the orientation tensor considering the direction of the coordinates as defined in Fig. 22.9 for “standard” specimen determined by CT

Tensor component	0°-position	90°-position	Knit line	Notch
X	0.200	0.406	0.468	0.373
Y	0.086	0.136	0.141	0.102
Z	0.714	0.458	0.391	0.524

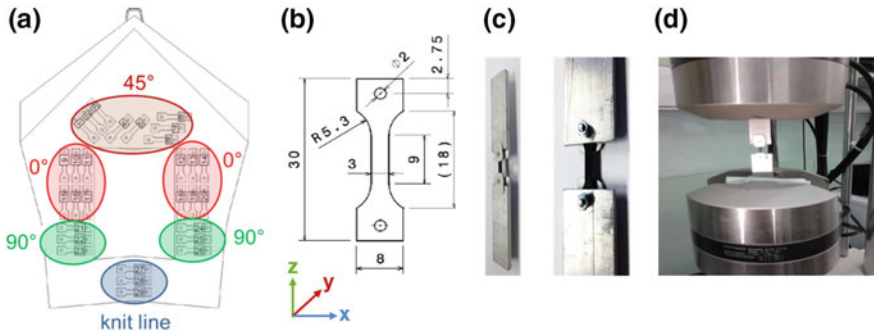


Fig. 22.10 Places of sampling of the “mini” specimen (a), dimensions of all “mini” specimen (b), fixing device for these specimen types (c), mounted “mini” specimen between the testing machine grips (d)

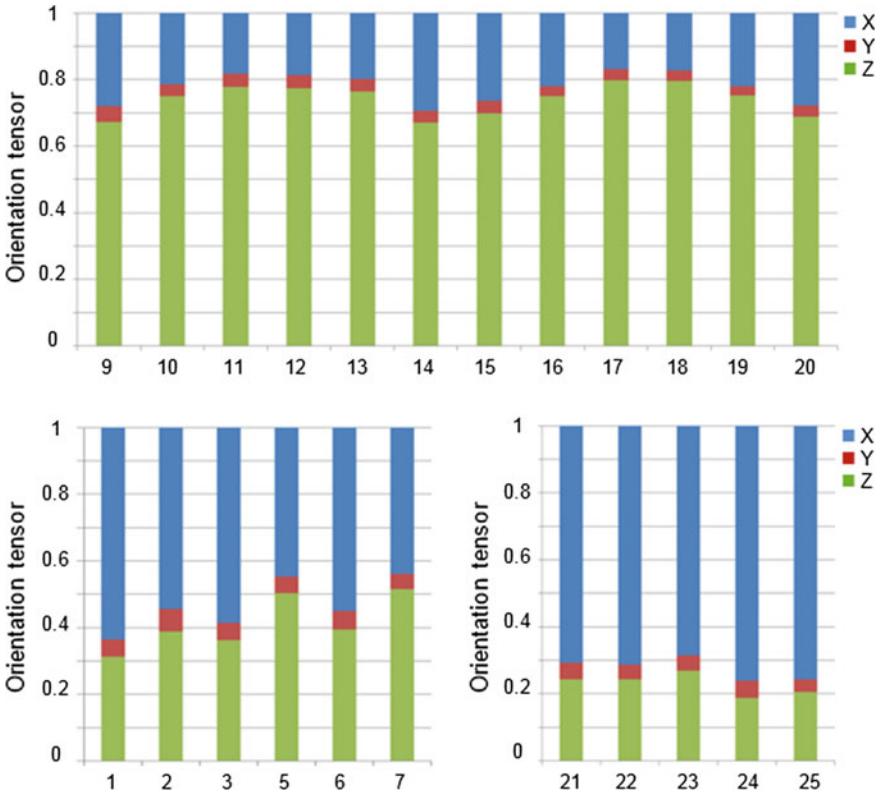


Fig. 22.11 Main diagonal components of the orientation tensor considering the direction of the coordinates as defined in Fig. 22.1 for the 0° (top), 45° (lower left) and 90° (lower right) “mini” specimen determined by CT

the tensor components for three layers (top, middle, bottom layer) of a 0° “mini” specimen.

The cyclic behaviour of glass fibre-reinforced thermoplastics is influenced by a number of different parameters [41, 42]. Main parameters are certainly the morphology of the material and the shape of the prepared specimen [14]. Also material anomalies like notches or knit lines have an impact on the fatigue behaviour. The other main parameters are loading factors like load type (tensile, compression, bending) [43], load profile (sine, rectangle, triangle), testing frequency [44, 45], thermal influence [46, 47] and other environmental effects.

Since fatigue strength is directly proportional to the tensile strength, tensile tests have been executed in advance of fatigue tests for a basic mechanical characterisation. Figure 22.12 shows load–elongation curves for the different specimen positions of the “standard” specimen. These results generated the basis for the following fatigue tests.

To characterise the fatigue behaviour a sinusoidal pulsating tensile loading was used for the load controlled testing. All results were obtained by a testing frequency of 10 Hz with $R = 0.1$ under room temperature. Only for the recording of high-speed images a cold-light source stressed the samples, though the light impulse lasted less than one second at each shot, there was no significant impact on the fatigue behaviour. The setup for the fatigue testing is shown in Fig. 22.13.

For the specification of materials fatigue behaviour commonly Wöhler curves were used, where strain is plotted against the number of cycles at fracture. Theoretical concepts for different loading types, the experimental planning and implementation of generating such curves are well known [41, 42, 48].

The generated Wöhler curves on the left side of Fig. 22.14 shows actually an expectable behaviour of the tested “standard” specimen. With the determined orientation tensors of the specimen positions, it was obvious that the 0° -position with a preferred fibre orientation parallel to the loading direction must perform best. Very similar results to these Wöhler curves have been made for other fibre-reinforced polymers [3–5]. The standardised Wöhler curves on the right side of Fig. 22.14 certify the proportionality of tensile and fatigue strength. It fits very well for the 0° - and notch-position. Only for the knit line a significant higher level and therefore a better fatigue behaviour related to the tensile behaviour compared with the usual characteristics of this polymer could be observed.

Table 22.4 Main diagonal components of the orientation tensor considering the direction of the coordinates as defined in Fig. 22.10b for a 0° “mini” specimen for three different layers determined by CT

Tensor component	Top	Middle	Bottom	Mean
X	0.22	0.18	0.21	0.20
Y	0.06	0.11	0.06	0.08
Z	0.72	0.71	0.73	0.72

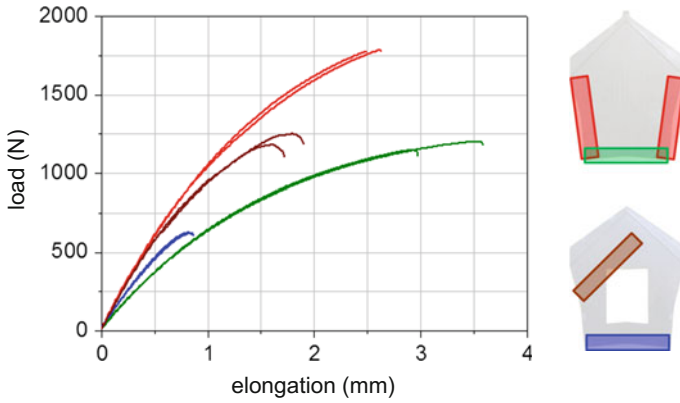


Fig. 22.12 Load–elongation curves for the different specimen positions

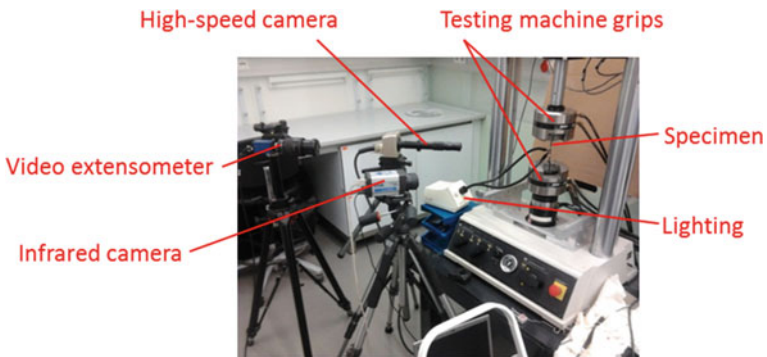


Fig. 22.13 Setup for fatigue testing with the different measurement systems

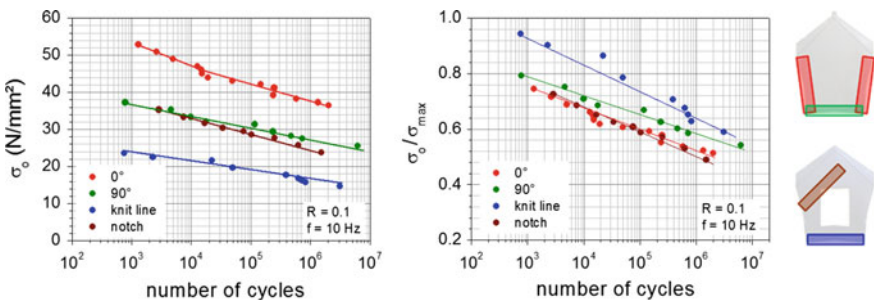


Fig. 22.14 Wöhler curves of the different positions of the “standard”-specimen (left) and normalised Wöhler curves of the same positions (right)

Plotting fatigue strength versus fibre orientation, represented by the main component of the orientation tensor parallel to loading direction shows a strong correlation (Fig. 22.15). The samples taken from the knit line and the notch region do not follow this correlation. In these regions the situations are more complex. For example in the notch region there is a strong stress concentration, which will lead to smaller values of fatigue strength.

For the durability analysis and the intended lifetime prediction several approaches were applied. Some of the used measurement equipment is illustrated in Fig. 22.13. Strain measurements are a main indication for the assessment of the fatigue status. Therefore strain was measured on different scales. By analysing the displacement of the testing machine grips a mean fatigue status over the entire specimen could be achieved. With the application of a video extensometer a more localised area near the place of the fracture was observable. For local strain measurements the installation of a high-speed camera in combination with digital image correlation was applied. Figure 22.16 shows strain measurement results of a knit-line specimen. The strain progression is quite continuous and shows equable fatigue behaviour also for different loadings.

By using the strain measurement results, a conventional analysis method is the investigation of energy dissipation and its changes with cumulative progress of the fatigue testing [11, 12]. The energy dissipation is determinable by calculating the area of the loading-based appearing hysteresis loops. Changes of size and shape or slope of the loops characterises the fatigue progress.

Results of a 0°-“standard” specimen show Fig. 22.17. The decrease of energy dissipation in the very beginning of the testing might be reasoned by an initial transient effect. Thereafter no significant change of size or slope could be obtained until shortly before break.

Another common approach is the analysis of the modulus [6, 7]. The development of the normalised modulus (E_N/E_0) shows Fig. 22.18. Compared to the

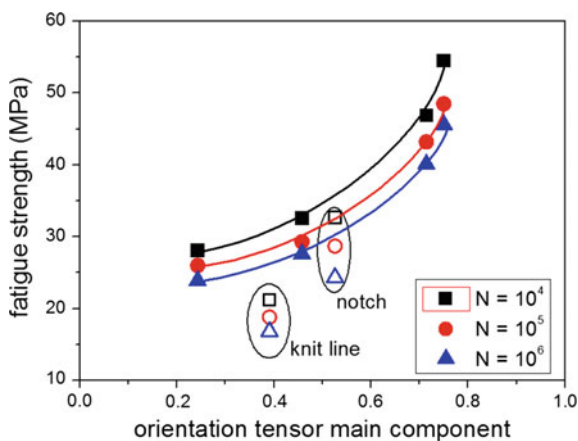


Fig. 22.15 Fatigue strength versus fibre orientation

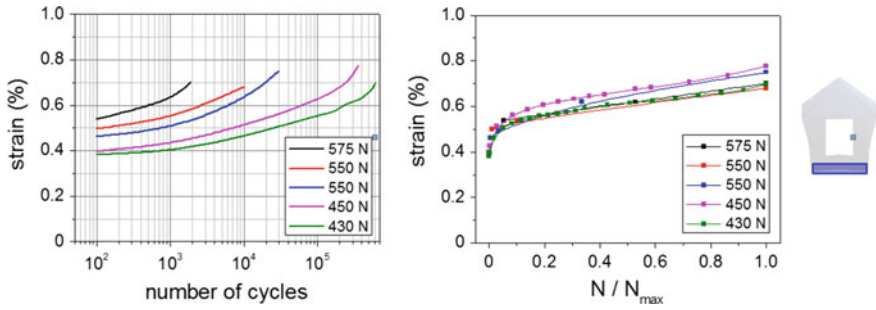


Fig. 22.16 Standardised strain against number of cycles (*left*) and lifetime progress (*right*) for a knit-line “standard” specimen measured with grip displacement method

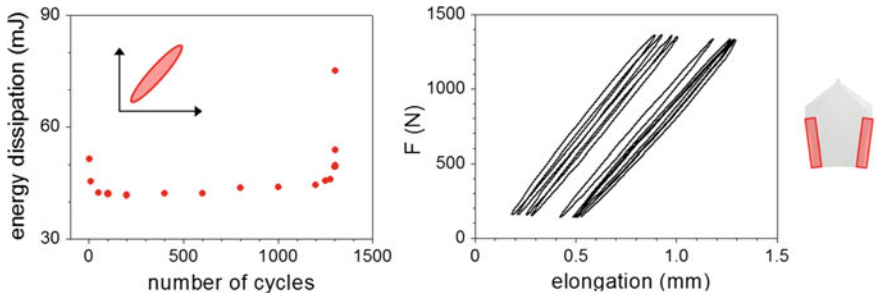


Fig. 22.17 Energy dissipation at different stages of cyclic loading (*left*) and the related hysteresis loops (*right*) for a 0°-“standard” specimen test

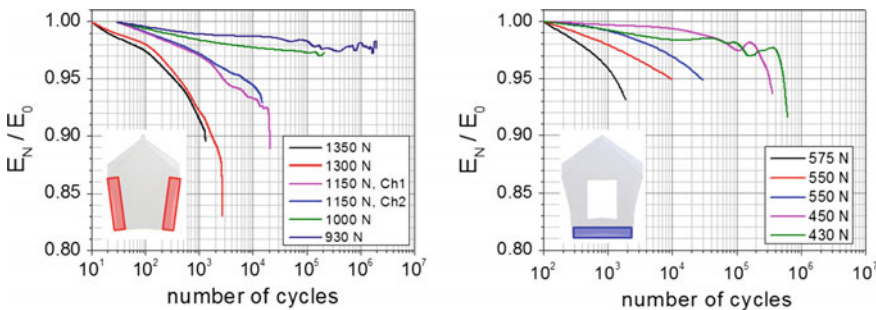


Fig. 22.18 Development of the normalised modulus (E_N/E_0) for a 0° (*left*) and a knit-line (*right*) “standard” specimen for different loadings

0°-position the specimen from the knit-line showed only a slight decline of the modulus, though occasionally there is an intermediate increase observable especially at higher loadings.

Besides the mechanical also temperature analysis methods were applied. An established approach is the measurement of the surface temperature with infrared cameras [7, 8]. The measured temperature development (see Fig. 22.19) corresponds quite well with the characteristic parameters of the mechanical analysis most notably with the energy dissipation. It seems that there are three stages in the progression of the surface temperature during the loading. After a rapid increase in the very beginning, a stage of constant temperature respectively continuous increase of the temperature (depending on the loading) lasting almost to the end of fatigue life appears. Also in the temperature progression a steep rise is observable not until the last cycles of the fatigue loading.

In general the achieved results with all that different analysis approaches gives no possibilities for a reliable lifetime prediction or the ability of an estimation of the actual fatigue status. There are no clear signs of damage until shortly before the fracture. For this reason the determination of local strain by digital image correlation was applied. Therefore the specimens are observed with a high-speed camera. Thus the maximum elongations at different progress of fatigue life could be determined even with unchanged testing frequency. A dot pattern is sprayed on the specimen. By analysing the local changes of this pattern, the local deformations could be visualised.

The progression of the local strain illustrated in Fig. 22.20 shows the advantage of this method. Very often there is an indication of the position of the later crack initiation visible in early stages of the fatigue testing. Sometimes these positions can be correlated to fibre clusters or slight surface imperfections. However an estimation of the actual fatigue life status is so far also with this method impossible. For this purpose the application of acoustic emission equipment appears promising.

One important task of evaluating the fatigue behaviour of SFRP parts is the modelling of fatigue damage accumulation and the prediction of lifetime under cyclic loading conditions. An overview on different approaches is given in [2].

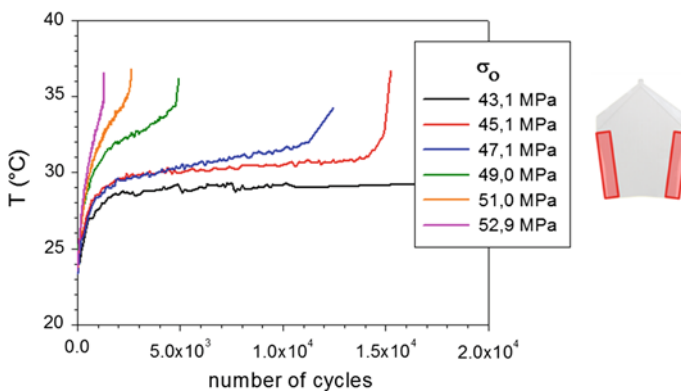


Fig. 22.19 Surface temperature as a function of the number of fatigue cycles of a 0°-“standard” specimen measured with IR-cameras for different loadings

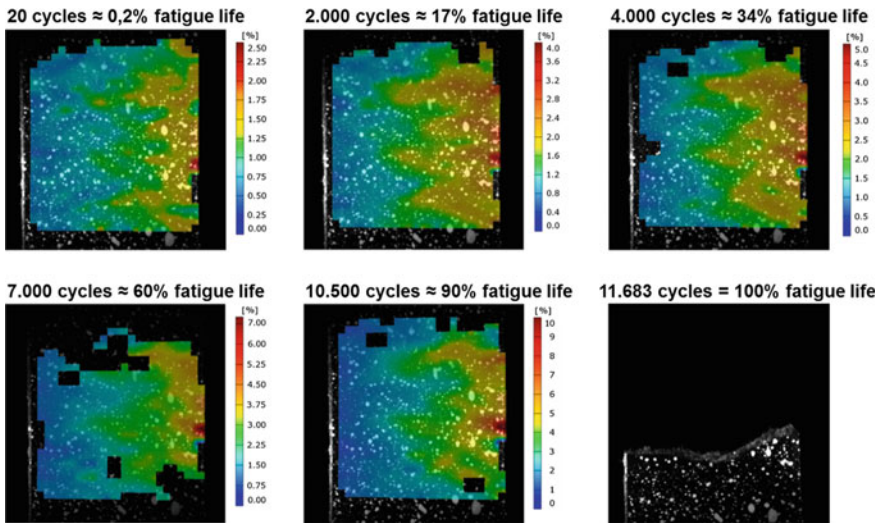


Fig. 22.20 Development of local strain fields obtained by digital image correlation for 90°-“standard” specimen loaded with $\sigma_0 = 32$ MPa

Evolutions of size or slope of the hysteretic loop, the non-linear viscoelastic part, the strain energy density and energy dissipation are suitable methods to describe the effects of cyclic loading on the lifetime [2]. To predict the lifetime of injection moulded industrial parts the knowledge of fibre orientations and of local load distribution during application is required. The combination of injection moulding simulation, morphology analysis, cyclic testing and numerical analysis can help to understand, forecast and optimise the fatigue resistance of complex parts. In principle there are two possibilities for numerical analysis: single-fibre approach and continuums mechanics approach. In [49] a micromechanical model for the fibre–matrix interface damages and matrix degradation due to fatigue loading is presented. It consists of a fracture mechanics-based description of fibre debonding, a crack growth rate based approach of the composites fatigue behaviour and a Wöhler valuation for quantification of the matrix damage.

References

1. Bierögel, C., Grellmann, W.: Fatigue loading. In: Grellmann, W., Seidler, S. (eds.) Landolt-Börnstein, New Series Volume VIII/6A3 Mechanical and Thermomechanical Properties of Polymers. Springer, Berlin (2014), Chapter 4.5, pp. 241–285
2. Mortazavian, S., Fatemi, A.: Fatigue behavior and modeling of short fiber reinforced polymer composites: A literature review. *Int. J. Fatigue* **70**, 297–321 (2015)

3. Zhou, Y., Mallick, P.K.: Fatigue performance of an injection-molded short E-glass fiber-reinforced polyamide 6.6. I. Effects of orientation, holes, and weld line. *Polym. Compos.* **27**, 230–237 (2006)
4. Cosmi, F., Bernasconi, A.: Fatigue Behaviour of Short Fibre Reinforced Polyamide: Morphological and Numerical Analysis of Fibre Orientation Effects. *Forni di Sopra* (2010), pp. 239–242
5. Bernasconi, A., Davoli, P., Basile, A., Filippi, A.: Effect of fibre orientation on the fatigue behaviour of a short glass fibre reinforced polyamide-6. *Int. J. Fatigue* **29**, 199–208 (2007)
6. Arif, M.F., Saintier, N., Meraghni, F., Fitoussi, J., Chemisky, Y., Robert, G.: Multiscale fatigue damage characterization in short glass fiber reinforced polyamide-66. *Compos. B* **61**, 55–65 (2014)
7. Esmaeillou, B., Fitoussi, J., Lucas, A., Tcharkhtchi, A.: Multi-scale experimental analysis of the tension-tension fatigue behavior of a short glass fiber reinforced polyamide composite. *Procedia Eng.* **10**, 2117–2122 (2011)
8. Bernasconi, A., Cosmi, F., Taylor, D.: Analysis of the fatigue properties of different specimens of a 10% by weight short glass fibre reinforced polyamide 6.6. *Polym. Test.* **40**, 149–155 (2014)
9. Bernasconi, A., Conrado, E., Hine, P.: An experimental investigation of the combined influence of notch size and fibre orientation on the fatigue strength of a short glass fibre reinforced polyamide 6. *Polym. Test.* **47**, 12–21 (2015)
10. Launay, A., Marco, Y., Maitournam, M.H., Raoult, I., Szmytka, F.: Cyclic behavior of short glass fiber reinforced polyamide for fatigue life prediction of automotive components. *Procedia Eng.* **2**, 901–910 (2010)
11. Pegoretti, A., Riccò, T.: Fatigue crack propagation in polypropylene reinforced with short glass fibres. *Compos. Sci. Technol.* **59**, 1055–1062 (1999)
12. Meneghetti, G., Ricotta, M., Lucchetta, G., Carmignato, S.: An hysteresis energy-based synthesis of fully reversed axial fatigue behaviour of different polypropylene composites. *Compos. B* **65**, 17–25 (2014)
13. Pegoretti, A., Ricco, T.: Crack growth in discontinuous glass fibre reinforced polypropylene under dynamic and static loading conditions. *Compos. A* **33**, 1539–1547 (2002)
14. Palmstingl, M., Koch, T., Salaberger, D., Paier, T.: Morphological impact on the fatigue behaviour of short fibre reinforced polypropylene. *Mater. Sci. Forum* **825–826**, 830–837 (2015)
15. Guild, F.J., Summerscales, J.: Microstructural image analysis applied to fibre composite materials: a review. *Composites* **24**, 383–393 (1993)
16. Salaberger, D., Kannappan, K.A., Kastner, J., Reussner, J., Auinger, T.: Evaluation of computed tomography data from fibre reinforced polymers to determine fibre length distribution. *Int. Polym. Proc.* **26**, 283–291 (2011)
17. Bay, R.S., Tucker III, C.L.: Stereological measurement and error estimates for three-dimensional fiber orientation. *Polym. Eng. Sci.* **32**, 240–253 (1992)
18. Bechtold, G., Gaffney, K.M., Botsis, J., Friedrich, K.: Fibre orientation in an injection moulded specimen by ultrasonic backscattering. *Compos. Part A: Appl. Sci. Manuf.* **29A**, 743–748 (1998)
19. Clarke, A.R., Archenhold, G., Davidson, N.C.: A novel technique for determining the 3D spatial distribution of glass fibres in polymer composites. *Compos. Sci. Technol.* **55**, 75–91 (1995)
20. Eberhardt, C., Clarke, A.: Fibre-orientation measurements in short-glass-fibre composites. Part I: automated, high-angular-resolution measurement by confocal microscopy. *Compos. Sci. Technol.* **61**, 1389–1400 (2001)
21. Yaguchi, H., Hojo, H., Lee, D.G., Kim, E.G.: Measurement of planar orientation of fibers for reinforced thermoplastics using image processing. *Int. Polym. Proc.* **10**, 262–269 (1995)
22. Kim, E.G., Park, J.K., Job, S.H.: A study on fiber orientation during the injection molding of fiber-reinforced polymeric composites (comparison between image processing results and numerical simulation). *J. Mater. Process. Technol.* **111**, 225–232 (2001)

23. Fakirov, S., Fakirova, C.: Direct determination of the orientation of short glass fibers in an injection-molded poly(ethylene terephthalate) system. *Polym. Compos.* **6**, 41–46 (1985)
24. Fisher, G., Eyerer, P.: Measuring spatial orientation of short fiber reinforced thermoplastics by image analysis. *Polym. Compos.* **9**, 297–304 (1988)
25. O'Connell, P.A., Duckett, R.A.: Measurements of fibre orientation in short-fibre-reinforced thermoplastics. *Compos. Sci. Technol.* **42**, 329–347 (1991)
26. Vincent, M., Giroud, T., Clarke, A., Eberhardt, C.: Description and modeling of fiber orientation in injection molding of fiber reinforced thermoplastics. *Polymer* **46**, 6719–6725 (2005)
27. Mönnich, S., Glöckner, R., Becker, F.: Analysis of fibre orientation using μ CT data. In: *Proceedings of 8th European LS-DYNA Conference (Strasbourg, 23/24.05.2011)*. Strasbourg (2011), 15 pages
28. Bernasconi, A., Cosmi, F., Hine, P.J.: Analysis of fibre orientation distribution in short fiber reinforced polymers: a comparison between optical and tomographic methods. *Compos. Sci. Technol.* **72**, 2002–2008 (2012)
29. Eberhardt, C., Clarke, A., Vincent, M., Giroud, T., Flouret, S.: Fibre-orientation measurements in short-glass-fibre composites—II: A quantitative error estimate of the 2D image analysis technique. *Compos. Sci. Technol.* **61**, 1961–1974 (2001)
30. Fu, S.-Y., Mai, Y.-W., Ching, E.C.-Y., Li, R.K.Y.: Correction of the measurement of fiber length of short fiber reinforced thermoplastics. *Compos. A* **33**, 1549–1555 (2002)
31. Pesendorfer, H.: *Morphologische Analyse von Faserverbunden mittels Schliiffverfahren*. Master thesis, TU Wien, Vienna (2015)
32. Advani, S.G., Tucker III, C.L.: The use of tensors to describe and predict fiber orientation in short fiber composites. *J. Rheol.* **31**, 751–784 (1987)
33. Mlekusch, B., Lehner, E.A., Geymayer, W.: Fibre orientation in short-fibre-reinforced thermoplastics I. Contrast enhancement for image analysis. *Compos. Sci. Technol.* **59**, 543–545 (1999)
34. Vélez-García, G.M., Wapperom, P., Kunc, V., Baird, D.G., Zink-Sharp, A.: Sample preparation and image acquisition using optical-reflective microscopy in the measurement of fiber orientation in thermoplastic composites. *J. Microsc.* **248**, 23–33 (2012)
35. Zhu, Y.T., Blumenthal, W.R., Lowe, T.C.: Determination of non-symmetric 3-D fiber-orientation distribution and average fiber length in short-fiber composites. *J. Compos. Mater.* **31**, 1287–1302 (1997)
36. Zak, G., Haberer, M., Park, C.B., Benhabib, B.: Estimation of average fibre length in short-fibre composites by a two-section method. *Compos. Sci. Technol.* **60**, 1763–1772 (2000)
37. Thomason, J.L.: The influence of fibre length and concentration on the properties of glass fibre reinforced polypropylene: 5. Injection moulded long and short fibre PP. *Compos. A Appl. Sci. Manuf.* **33**, 1641–1652 (2002)
38. Bernasconi, A., Cosmi, F., Dreossi, D.: Local anisotropy analysis of injection moulded fibre reinforced polymer composites. *Compos. Sci. Technol.* **68**, 2574–2581 (2008)
39. Köpplmayr, T., Milosavljevic, I., Aigner, M., Hasslacher, R., Plank, B., Salaberger, D., Miethlinger, J.: Influence of fiber orientation and length distribution on the rheological characterization of glass-fiber-filled polypropylene. *Polym. Test.* **32**, 535–544 (2013)
40. Gupta, V.B., Mittal, R.K., Sharma, P.K., Menning, G., Wolters, J.: Some studies on glass fiber-reinforced polypropylene. Part I: Reduction in fiber length during processing. *Polym. Compos.* **10**, 8–15 (1989)
41. Oberbach, K.: Untersuchung des Dauerschwingverhaltens. In: Carlowitz, B. (Ed.): Band 1. *Die Kunststoffe. Chemie, Physik, Technologie*. In: Becker, G. W., Braun D. (Eds.): *Kunststoff-Handbuch*. Carl Hanser, Munich (1990), Chapter 5.3.3, pp. 659–686
42. Höniger, H.: Fatigue behavior. In: Grellmann, W., Seidler, S. (eds.): *Polymer Testing*, 2nd edn. Carl Hanser, Munich (2013), Chapter 4.5, pp. 161–170
43. Domininghaus, H.: *Plastics for Engineers. Materials, Properties, Applications*. Carl Hanser, Munich (1993)

44. Hertzberg, R.W., Manson, J.A., Skibo, M.: Frequency sensitivity of fatigue processes in polymeric solids. *Polym. Eng. Sci.* **15**, 252–260 (1975)
45. Pegoretti, A., Ricco, T.: Crack growth in discontinuous glass fibre reinforced polypropylene under dynamic and static loading conditions. *Compos. A* **33**, 1539–1547 (2002)
46. Kurashiki, K., Ni, Q.-Q., Maesaka, T., Iwamoto, M.: A study on evaluation of fatigue damage of GFRP by infrared thermography. 1st report. Fatigue temperature rise curves of GFRP. *Trans. Jpn. Soc. Mech. Eng. A* **66**, 960–965 (2000)
47. Katunin, A.: Thermal fatigue of polymeric composites under repeated loading. *J. Reinf. Plast. Compos.* **31**, 1037–1044 (2012)
48. Ehrenstein, G.W.: *Faserverbund-Kunststoffe. Werkstoffe, Verarbeitung, Eigenschaften*. Carl Hanser, Munich (2006)
49. Brighenti, R., Carpinteri, A., Scorza, D.: Micromechanical crack growth-based fatigue damage in fibrous composites. *Int. J. Fatigue* **82**, 98–109 (2016)